COMPUTATION OF EIGENMODES IN THE BESSY VSR CAVITY CHAIN BY MEANS OF CONCATENATION STRATEGIES*

Thomas Flisgen[†], Adolfo Vélez

Helmholtz-Zentrum Berlin für Materialien und Energie GmbH (HZB), 12489 Berlin, Germany

Johann Heller, Shahnam Gorgi Zadeh, and Ursula van Rienen

Institute of General Electrical Engineering, University of Rostock, 18059 Rostock, Germany

Abstract

The computation of eigenmodes in chains of superconducting cavities with asymmetric couplers is a demanding problem. This problem typically requires the use of high-performance computers in combination with dedicated software packages. Alternatively, the eigenmodes of chains of superconducting cavities can be determined by the so-called State-Space Concatenation (SSC) approach that has been developed at the University of Rostock. SSC is based on the decomposition of the full chain into individual segments. Subsequently, the RF properties of every segment are described by reduced-order models. These reduced-order models are concatenated to a reduced-order model of the entire chain by means of algebraic side constraints arising from continuity conditions of the fields across the decomposition planes. The constructed reduced-order model describes the RF properties of the complete structure so that the field distributions, the coupling impedances and the external quality factors of the eigenmodes of the full cavity chain are available. In contrast to direct methods, SSC allows for the computation of the eigenmodes of cavity chains using desktop computers. The current contribution revises the scheme using the BESSY VSR cavity chain as an example. In addition, a comparison between a direct computation of a specific localized mode is described.

INTRODUCTION

The computation of eigemodes of superconducting RF resonators used for the acceleration of charged particles is a standard task in computational accelerator physics. Complementary to the characterization of the accelerating mode, higher-order modes are of special interest as they can interact with the beam as well and may lead to additional cryogenic load or beam instabilities. Often eigenmode computations are restricted to single cavities with couplers to reduce computational efforts, despite the fact that the cavities are arranged in chains and are connected via the beam pipes. These chains are accommodated in cryomodules providing the cryogenic infrastructure to cool the resonators so that their surfaces become superconducting.

The consideration of single cavities with couplers is a reasonable approximation for characterizing the accelerating mode as the field distribution of this mode is on purpose confined in the cavity. However, the restriction to a single cavity often becomes invalid for higher-order modes, in particular if mode resonant frequencies are larger than the fundamental cutoff frequency of the beam pipe connecting the adjacent cavities. The field distributions of higher-order modes in cavity chains are much more complex than in single cavities as the fields can be distributed along the entire cavity chain or along parts of it.

Direct approaches to determine the eigenmode spectrum of cavity chains require high-performance computers [1–4]. Alternatively, the State-Space Concatenation (SSC) [5–9] approach allows for computing the eigenmodes in complex chains of cavities with asymmetric couplers using desktop computers. The scheme is based on decomposing the complex cavity chain into segments. The electromagnetic fields of the segments are described using state-space equations (coupled systems of ordinary differential equations) obtained from analytical calculations or from numerical discretization techniques such as the Finite-Integration Technique [10, 11]. Typically, the aforementioned state-space equations have many degrees of freedom to account for the distributed nature of the underlying partial differential equations. Fortunately, the number of degrees of freedom for each state-space model can be significantly reduced using model-order reduction (MOR) approaches [12–14]. Subsequently, all reduced-order models are concatenated by means of algebraic side constraints, which ensure that the tangential electric and magnetic fields are continuous across the surfaces of the decomposition planes. This concatenation delivers a very compact description of the complex structure in terms of its electromagnetic properties and allows for the determination of its eigenmodes by computing the eigenvalues and eigenvectors of comparably small matrices.
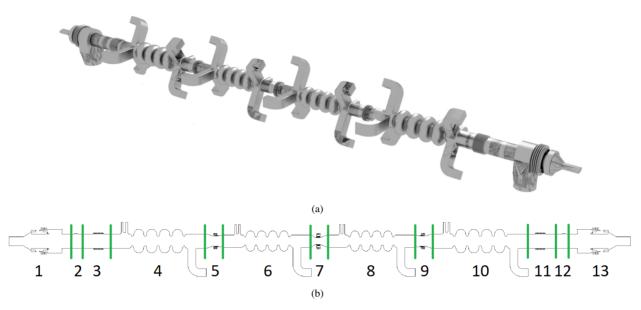
In this paper, the SSC scheme is revised using the BESSY VSR chain of superconducting cavities as an application example. The presented work has been conducted in the framework of a collaboration between the University of Rostock and the Helmholtz-Zentrum Berlin. Predominantly, this article is based on the internal report [15], which comprises all details of the computations. The field patterns and properties of the computed eigenmodes are listed in a compendium attached to [15]. All computations for the internal report have been conducted by J. Heller. In addition to the results provided by the internal report, this article presents a comparison between results from SSC and a direct computation using CST Studio Suite® (CST) [16]. Note that

Figure 1: (a) Geometry of the BESSY VSR cavity string. Its main components are two cavities whose TM_{01}-π-modes resonate at 1.5 GHz and two cavities whose TM_{01}-π-modes resonate at 1.75 GHz. All cavities are constructed by means of ellipses. The 1.5 GHz cavities are located at both ends of the chain whereas the 1.75 GHz cavities are in between. Each cavity is equipped with one fundamental power coupler and five waveguides for the absorption of higher-order modes. At both ends of the complete chain endgroups with tapers, bellows, pump domes and dielectric absorbers are located. The figure is adapted from [15]. (b) Decomposition of the chain of cavities into individual segments. The green lines denote the decomposition planes. The arising segments are: 1. endgroup, 2. valve, 3. bellow, 4. cavity (1.5 GHz), 5. shielded bellow, 6. cavity (1.75 GHz), 7. collimating shielded bellow, 8. cavity (1.75 GHz), 9. shielded bellow, 10. cavity (1.5 GHz), 11. bellow, 12. valve, and 13. endgroup.

further comparisons between direct computations and SSC computations are available in [5, 6, 8, 9].

EIGENMODES OF THE BESSY VSR CHAIN USING SSC

The third generation light source BESSY II is operated by the Helmholtz-Zentrum at the Wilhelm-Conrad-Röntgen-Campus in Berlin Adlershof in Germany. BESSY II is a user facility providing photon pulses ranging from the Terahertz to the hard X-ray regime. Its main component is a ring with a circumference of 240 m which can store currents up to 300 mA with the energy of 1.7 GeV. Currently, the upgrade of BESSY II to BESSY VSR (Variable pulse-length Storage Ring) is in preparation. BESSY VSR allows for simultaneously storing long and short pulses in the machine [17–19].

The upgrade requires the insertion of a cryomodule accommodating two superconducting 1.5 GHz and two superconducting 1.75 GHz four-cell resonators into the existing BESSY II ring. Figure 1 depicts the layout of the string of superconducting cavities. The first and the last cavities in the string are constructed such that their TM_{01}-π-modes resonate with 1.5 GHz, whereas the two cavities in the center of the chain are designed so that their TM_{01}-π-modes resonate with 1.75 GHz. The four cavities in the BESSY VSR cavity chain are connected by means of bellows. The

chain is equipped with pump domes, dielectric absorbers, bellows and tapers at both ends. Please refer to Figure 2 in [20] for a detailed view of the endgroups.

The superposition of the accelerating fields of all four cavities depicted in Figure 1 results in a beating pattern. In fact, the derivative with respect to the longitudinal direction of the voltages cancels for every second bunch whereas for the remaining bunches the derivative of the voltages constructively is added up. Together with the optics of the machine, the voltage beating pattern leads to long and short pulses simultaneously stored in the ring.

Eigenmodes and their Properties

The electric fields $\mathbf{E}_n(\mathbf{r})$ of the eigenmodes in the cavity string fulfill Helmholtz equation

$$\Delta \mathbf{E}_n(\mathbf{r}) + \varepsilon \mu \omega_n^2 \, \mathbf{E}_n(\mathbf{r}) = \mathbf{0} \qquad (1)$$

with the boundary conditions

$$\mathbf{n} \times \mathbf{E}_n(\mathbf{r}) = \mathbf{0} \text{ on } \partial\mathbf{\Omega}_{\text{PEC}} \qquad (2)$$

and

$$\mathbf{n} \cdot \mathbf{E}_n(\mathbf{r}) = 0 \text{ on } \partial\mathbf{\Omega}_{\text{Port}}. \qquad (3)$$

Here, ε and μ denote the permittivity and the permeability of free space, respectively. The resonant angular frequency of the nth eigenmode is denoted by ω_n. Perfect electric

conducting boundary conditions are assumed on the boundary $\partial\Omega_{\text{PEC}}$ of the superconducting cavities, whereas perfect magnetic conducting boundary conditions are enforced on the boundary Ω_{Port} of the external waveguide ports. External waveguide ports are assigned at the beam pipe at both ends of the chain, at the ends of the fundamental power couplers and at the ends of the higher-order mode couplers.

In addition to the frequencies $f_n = \omega_n/2/\pi$ and the field distributions $\mathbf{E}_n(\mathbf{r})$ of the eigenmodes, their coupling impedances

$$\left(\frac{r}{Q}\right)_n = \frac{1}{\omega_n W_n}\left|\int_{z_{\min}}^{z_{\max}} E_{n,z}(x_0,y_0,z)\,\mathrm{e}^{j\omega_n z/c}\,\mathrm{d}z\right|^2 \quad (4)$$

are of special interest. Here, W_n denotes the energy stored in the nth eigenmode, $z_{\min}$ and $z_{\max}$ the beginning and the end of the chain in longitudinal direction, $E_{n,z}(x_0,y_0,z)$ the on-axis longitudinal component of the electric field of the nth eigenmode and $c = 1/\sqrt{\varepsilon\mu}$ the speed of light in vacuum.

Another important quantity related to resonant modes is the external quality factor defined by

$$Q_{\text{ext},n} = \frac{\omega_n W_n}{P_{\text{loss},n}}, \quad (5)$$

where $P_{\text{loss},n}$ is the propagation of energy through the open waveguide ports of the structure. Note that the external quality factors $Q_{\text{ext},n}$ do not directly result from Eqs. (1–3) because perfect magnetic boundary conditions are enforced on the port planes Ω_{Port}. Consequently, the Poynting vector normal to the port boundary equals zero. Nonetheless, $Q_{\text{ext},n}$ can be approximated from the lossless eigenmodes using a later described perturbation approach.

It is worth to note that the coupling impedance $(r/Q)_n$ specifies the coupling of the eigenmode with the bunch of charged particles, whereas the external quality factor $Q_{\text{ext},n}$ quantifies the coupling of the mode to the waveguide ports.

Decomposition of the Chain into Segments

In a first step, the BESSY VSR cavity chain is decomposed into individual segments. The decomposition planes are depicted in Figure 1(b) by green lines. In total, 13 segments are obtained. Following Figure 1(b) from the left to the right, the segments are endgroup, valve, bellow, cavity (1.5 GHz), shielded bellow, cavity (1.75 GHz), collimating shielded bellow, cavity (1.75 GHz), shielded bellow, cavity (1.5 GHz), bellow, valve, and endgroup. Note that the decomposition planes are chosen at regions of constant cross section to keep the number of 2D port modes required for the field expansion in the cut planes small. To each 2D port mode a modal voltage corresponding to the electric field distribution of the port mode and a modal current corresponding to the magnetic field distribution of the port mode are assigned. It is distinguished between internal ports located at the cutplanes arising from the decomposition and external ports located at the ends of the beam pipe or at ends of power and higher-order mode couplers. Depending on the cross section of the cutplanes 8, 16, or 20 2D port

modes are considered for the field expansion in these planes. Consequently, 8, 16, or 20 modal voltages and currents are required per cutplane per segment. Please refer to column five in Table 3.1 in [15] for more details.

Electromagnetic Properties of the Segments

To describe the electromagnetic properties of the $R = 13$ segments, each substructure is discretized by means of a hexahedral mesh using the commercial software CST [16]. Subsequently, the discrete wave equation with excitation is exported to MATLAB [21], so that the second-order state-space systems

$$\frac{\mathrm{d}^2}{\mathrm{d}t^2}\mathbf{x}_r(t) = \mathbf{A}_r\,\mathbf{x}_r(t) + \mathbf{B}_r\,\frac{\mathrm{d}}{\mathrm{d}t}\mathbf{i}_r(t) \quad (6)$$

are available for each segment. Here, $1 \le r \le R$ is the segment index, $\mathbf{x}_r(t) \in \mathbb{R}^{N_d}$ is a time-dependent state vector, $\mathbf{A}_r \in \mathbb{R}^{N_d \times N_d}$ the system matrix, $\mathbf{B}_r \in \mathbb{R}^{N_d \times N_t}$ the input matrix, and $\mathbf{i}_r(t) \in \mathbb{R}^{N_t}$ the time-dependent excitation term. The excitation term comprises modal port currents of the waveguide ports of the rth segment. In close analogy, the vector

$$\mathbf{v}_r(t) = \mathbf{B}_r^{\mathrm{T}}\,\mathbf{x}_r(t) \quad (7)$$

lists the time-dependent modal voltages of the rth segment. The total number of 2D port modes of each segment is given by N_t.

Following the Finite-Integration Technique (FIT) [10, 11], the state matrix can be chosen to be

$$\mathbf{A}_r = -\mathbf{M}_{\varepsilon,r}^{-1/2}\mathbf{C}_r^{\mathrm{T}}\mathbf{M}_{\mu,r}^{-1}\mathbf{C}_r\mathbf{M}_{\varepsilon,r}^{-1/2}, \quad (8)$$

where the discrete representation of the curl operator is denoted by $\mathbf{C}_r$. The matrices $\mathbf{M}_{\varepsilon,r}$ and $\mathbf{M}_{\mu,r}$ are diagonal and comprise properties of the grid and averaged material parameters. The input matrix (or output matrix transposed) is given by

$$\mathbf{B}_r = \mathbf{M}_{\varepsilon,r}^{-1/2}\mathbf{R}_r. \quad (9)$$

The columns of the matrix $\mathbf{R}_r$ comprise the electric field distributions of the 2D port modes in a lexicographic order. Note that the sampled 3D electric field distribution in the rth segment is given in a lexicographic order by

$$\mathbf{e}_r(t) = \mathbf{D}_{s,r}^{-1}\mathbf{M}_{\varepsilon,r}^{-1/2}\mathbf{x}_r(t), \quad (10)$$

where $\mathbf{D}_{s,r}$ is a diagonal matrix holding the lengths of the edges of the primary grid.

Model-Order Reduction

The number of degrees of freedom of each state-space model can be significantly reduced by means of model-order reduction approaches. The reduction is conducted by expressing a reduced state vector $\mathbf{x}_{\text{rd},r}(t) \in \mathbb{R}^{N_{\text{dr}}}$ using a semi-orthogonal reduction matrix $\mathbf{W}_r \in \mathbb{R}^{N_d \times N_{\text{dr}}}$:

$$\mathbf{x}_r(t) = \mathbf{W}_r\,\mathbf{x}_{\text{rd},r}(t). \quad (11)$$

TUPAG01

As a matter of fact, there are various ways to construct the reduction matrix. In the framework of this study, a proper orthogonal decomposition is used which requires a finite set of frequency-domain field distributions of the state-space space system Eq. (6). It is a key property that the reduction matrix has much more rows than columns, i.e. $N_\mathrm{d} \gg N_\mathrm{dr}$. Replacing Eq. (11) in Eq. (6) and multiplying the obtained equation with $\mathbf{W}_r^\mathrm{T}$ from the left hand side gives

$$\frac{\mathrm{d}^2}{\mathrm{d}t^2}\mathbf{x}_{\mathrm{rd},r}(t) = \underbrace{\mathbf{W}_r^\mathrm{T}\mathbf{A}_r\mathbf{W}_r}_{\mathbf{A}_{\mathrm{rd},r}}\ \mathbf{x}_{\mathrm{rd},r}(t) + \underbrace{\mathbf{W}_r^\mathrm{T}\mathbf{B}_r}_{\mathbf{B}_{\mathrm{rd},r}}\ \frac{\mathrm{d}}{\mathrm{d}t}\mathbf{i}_r(t) \quad (12)$$

on account of the semi-orthogonality of the reduction matrix ($\mathbf{W}_r^\mathrm{T}\mathbf{W}_r = \mathbf{I}$).

Replacing Eq. (11) in Eq. (7) delivers the reduced-order output equation

$$\mathbf{v}_r(t) = \underbrace{\mathbf{B}_r^\mathrm{T}\mathbf{W}_r}_{\mathbf{B}_{\mathrm{rd},r}^\mathrm{T}}\ \mathbf{x}_{\mathrm{rd},r}(t). \quad (13)$$

For instance, the model-order reduction allows for reducing the number of degrees of freedom from $N_\mathrm{d} \approx 5.5 \times 10^6$ to $N_\mathrm{dr} \approx 9.2 \times 10^2$ for the 1.5 GHz cavities and from $N_\mathrm{d} \approx 5.5 \times 10^4$ to $N_\mathrm{dr} \approx 2.5 \times 10^2$ for the valves. Please refer to column three of Table 3.1 in [15] for the number of degrees of freedom for the remaining segments.

The computation of the reduction matrices was performed on an Intel(R) Xeon(R) CPU E5-2687W @ 3.4 GHz with 256 GB of RAM using Windows Server 2012. The total computation time to determine all reduction matrices based on an accuracy criterion was approximately 6 d and 2 h. Column nine of Table 3.1 in [15] presents the computing times for the construction of the reduction matrix for each of the $R = 13$ segments.

Concatenation of State-Space Models

To concatenate the reduced-order state-space models of the individual segments to a reduced-order state-space model of the full structure, all state-space models are collated in terms of a block system. For instance, this reads

$$\mathbf{x}_\mathrm{b}(t) = \left(\mathbf{x}_{\mathrm{rd},1}^\mathrm{T}(t)\ \mathbf{x}_{\mathrm{rd},2}^\mathrm{T}(t)\ \ldots\ \mathbf{x}_{\mathrm{rd},r}^\mathrm{T}(t)\ \ldots\ \mathbf{x}_{\mathrm{rd},R}^\mathrm{T}(t)\right)^\mathrm{T} \quad (14)$$

for the state vector of the block system. In a next step, this block system is modified to ensure that Kirchhoff's laws are fulfilled for modal voltages and modal currents of ports to be coupled. Following [6, Appendix C.2], Kirchhoff's laws result from continuity constraints of tangential electric and magnetic fields. The incorporation of Kirchhoff's laws into the block state-space system delivers a state-space system of the full structure. This system is again reduced to obtain

$$\frac{\mathrm{d}^2}{\mathrm{d}t^2}\mathbf{x}_\mathrm{cr}(t) = \mathbf{A}_\mathrm{cr}\mathbf{x}_\mathrm{cr}(t) + \mathbf{B}_\mathrm{cr}\frac{\mathrm{d}}{\mathrm{d}t}\mathbf{i}_\mathrm{ext}(t) \quad (15)$$

with the output equation

$$\mathbf{v}_\mathrm{ext}(t) = \mathbf{B}_\mathrm{cr}^\mathrm{T}\mathbf{x}_\mathrm{cr}(t). \quad (16)$$

This system is a very compact description of the electromagnetic properties of the BESSY VSR cavity chain. Note that the relationship between the reduced state-vector of the concatenated system and the state-vector of the block system is given by

$$\mathbf{x}_\mathrm{b}(t) = \mathbf{W}_\mathrm{c}\,\mathbf{x}_\mathrm{cr}(t), \quad (17)$$

with the semi-orthogonal reduction matrix $\mathbf{W}_\mathrm{c} \in \mathbb{R}^{6,921 \times 3,573}$ of the concatenated system.

Determination of Eigenmodes

As perfect magnetic conducting boundary conditions are assumed on the surfaces of the external waveguide ports

$$\mathbf{i}_\mathrm{ext}(t) = \mathbf{0} \quad (18)$$

is enforced for the eigenmode computations. Note that modal currents correspond to the tangential magnetic fields of the respective 2D port modes on the port surfaces. Using the constraint Eq. (18) and transforming the reduced-order state-equation Eq. (15) of the complete structure into frequency domain leads to the eigenvalue problem

$$\mathbf{A}_\mathrm{cr}\ \underbrace{\mathbf{x}_\mathrm{cr}}_{\mathbf{v}_{\mathrm{cr},n}} = \underbrace{-\omega^2}_{\lambda_n}\ \underbrace{\mathbf{x}_\mathrm{cr}}_{\mathbf{v}_{\mathrm{cr},n}}. \quad (19)$$

The eigenvectors $\mathbf{v}_{\mathrm{cr},n}$ as well as the eigenvalues are real-valued because of the symmetry of the matrix $\mathbf{A}_\mathrm{cr}$. A comparison of constants in Eq. (19) gives the following relation between resonant frequencies of the eigenmodes of the entire chain and the eigenvalues of the system matrix:

$$f_n = \frac{\omega_n}{2\pi} = \frac{1}{2\pi}\sqrt{-\lambda_n} \in \mathbb{R}. \quad (20)$$

The frequencies are real-valued, because λ_n is smaller than or equal to zero on account of the negative semi-definiteness of $\mathbf{A}_\mathrm{cr}$.

The field distributions of the nth eigenmode are determined based on the eigenvectors $\mathbf{v}_{\mathrm{cr},n}$. In a first step, the state-vector of the block system used for the concatenation is computed:

$$\mathbf{v}_{\mathrm{b},n} = \mathbf{W}_\mathrm{c}\mathbf{v}_{\mathrm{cr},n}. \quad (21)$$

Then, the vector $\mathbf{v}_{\mathrm{b},n}$ is partitioned following its definition in Eq. (14). Subsequently, the reduced-order state vectors $\mathbf{v}_{\mathrm{rd},r,n}$ of each segment are employed to reconstruct the electric field distribution of the nth mode in the rth segment:

$$\mathbf{e}_{r,n} = \mathbf{D}_{\mathrm{s},r}^{-1}\mathbf{M}_{\varepsilon,r}^{-1/2}\mathbf{W}_r\,\mathbf{v}_{\mathrm{rd},r,n}. \quad (22)$$

The sampled electric field distributions in $\mathbf{e}_{r,n}$ are stored in a lexicographic order and are transferred to a 3D field so that they can be exported to ParaView [22]. A processing script is used to automatically create field plots of all modes with resonant frequencies in the interval from 500 MHz to 3.6 GHz. The field plots show the absolute value of the electric fields in two different cutplanes. Based on the electric fields and the resonant frequencies, the coupling impedances $(r/Q)_n$ are also determined.

Determination of Quality Factors

The external quality factors of lossy modes in the BESSY VSR cavity chain are determined using a perturbation approach. In a first step, the state-space model Eqs. (15) and (16) of the lossless closed cavity chain is transferred to a model with first-order derivatives with twice as many states as the model with second-order derivatives:

$$\frac{\mathrm{d}}{\mathrm{d}t}\tilde{\mathbf{x}}_{\mathrm{cr}}(t) = \tilde{\mathbf{A}}_{\mathrm{cr}}\,\tilde{\mathbf{x}}_{\mathrm{cr}}(t) + \tilde{\mathbf{B}}_{\mathrm{cr}}\,\mathbf{i}_{\mathrm{ext}}(t) \qquad (23)$$

with the corresponding output equation

$$\mathbf{v}_{\mathrm{ext}}(t) = \tilde{\mathbf{B}}_{\mathrm{cr}}^{\mathrm{T}}\,\tilde{\mathbf{x}}_{\mathrm{cr}}(t). \qquad (24)$$

The matrices with the tilde directly result from the quantities without the tilde. To account for open boundary conditions, the external modal excitation currents are chosen based on the modal voltages in frequency domain:

$$\underline{\mathbf{i}}_{\mathrm{ext}}(j\omega) = -\underline{\mathbf{D}}_z^{-1}(j\omega)\,\underline{\mathbf{v}}_{\mathrm{ext}}(j\omega), \qquad (25)$$

whereas $\underline{\mathbf{D}}_z(j\omega)$ is the diagonal matrix holding the frequency-dependent wave impedances of the 2D ports modes at the external waveguide ports. Combining Eq. (25) with the state-space system Eq. (23) and Eq. (24) and transferring the resulting statement into frequency domain gives the nonlinear eigenvalue problem

$$\left[\tilde{\mathbf{A}}_{\mathrm{cr}} - \tilde{\mathbf{B}}_{\mathrm{cr}}^{\mathrm{T}}\,\underline{\mathbf{D}}_z^{-1}(\underbrace{j\underline{\omega}_n}_{\underline{\lambda}_n})\,\tilde{\mathbf{B}}_{\mathrm{cr}}\right]\underline{\tilde{\mathbf{x}}}_{\mathrm{cr},n} = \underbrace{j\underline{\omega}_n}_{\underline{\lambda}_n}\,\underline{\tilde{\mathbf{x}}}_{\mathrm{cr},n}. \qquad (26)$$
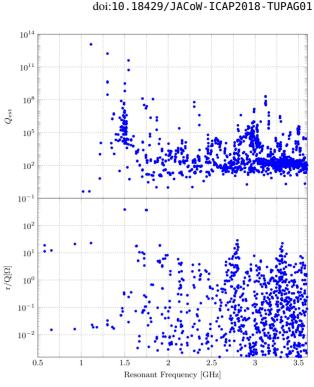
The reader is referred to [23, 24] for a complete description of the nonlinear eigenvalue problem arising from external quality factor computations. The frequencies of the lossy modes and their external quality factors are determined by

$$f_{\mathrm{ext},n} = \frac{\Im\{\underline{\lambda}_n\}}{2\pi}, \quad Q_{\mathrm{ext},n} = -\frac{\Im\{\underline{\lambda}_n\}}{2\Re\{\underline{\lambda}_n\}}. \qquad (27)$$

Note that the external quality factors are not directly linked to the lossless eigenmodes as the introduction of losses leads to a coupling of all eigenmodes. Consequently, the resonant frequencies and field distributions for lossy modes are different from lossless modes. Therefore, it is in general difficult to directly connect external quality factors to eigenmodes obeying Eq. (1) with the boundary conditions Eqs. (2) and (3).

NUMERICAL RESULTS

The central result of the described computations is a modal compendium listing the resonant frequencies, the coupling impedances, and the field distributions of 1,576 eigenmodes which were found in the interval 500 MHz to 3.6 GHz. The modal compendium is part of [15] and comprises a large variety of modes with complex field patterns such as cavity modes, multi-cavity modes, bellow modes or combinations of these. Note that the complete and rigorous

Figure 2: Semilog plots of the external quality factors (top) and the coupling impedances (bottom) of modes in the BESSY VSR cavity chain.

discussion of the results is not feasible on account of the large amount of generated data.

The diagram in the upper part of Figure 2 shows the external quality factors of modes in the BESSY VSR cavity chain. It is worth to mention that the modes with excessively large external quality factors ($10^{11}\ldots 10^{14}$) in the interval 578 MHz to 1.54 GHz are modes either being localized in the collimators or close to the dielectric absorbers. Both parts are assumed to be lossless in the computation, so that the quality factors of confined modes in these segments are estimated to be large. In practice however, these segments are not lossless so their quality factors are significantly reduced as factors of these modes are governed by dielectric and surface losses and not by external losses.

The diagram in the lower part of Figure 2 depicts the coupling impedances. The TM_{01}-π modes of the 1.5 GHz resonators and the 1.75 GHz resonators with their $(r/Q)_n$ in the order of $10^2\,\Omega$ are readily identifiable. On purpose, these modes have the largest coupling impedances. In addition to these modes, various modes with comparably large coupling impedances in the order of $1\,\Omega$ to $10\,\Omega$ exist. These modes are of potential danger for the operation of BESSY VSR, in particular, if their resonant frequencies are close to the $\Delta f = 250\,\mathrm{MHz}$ harmonics of the periodic BESSY VSR current. Please refer to Figure 3 in [20] for the spectrum of the BESSY VSR current.

For a review of the set of modes relevant for the operation of BESSY VSR, the reader is referred to [15]. The follow-
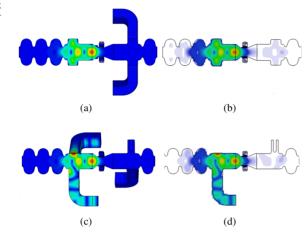
Figure 3: Absolute value of the electric field distribution of mode $n = 888$. The colorbar is presented in Figure 5(a). The field distribution is predominantly located in the waveguide connecting the cavity with the collimating shielded bellow and the higher-order mode waveguide absorber. The frequency of the mode is $f_{888}^{\mathrm{SSC}} = 2.9899\,\mathrm{GHz}$ and its coupling impedance is $(r/Q)_{888}^{\mathrm{SSC}} \approx 7.73\,\Omega$.

Figure 4: Electric field distribution of mode $n = 888$ on orthogonal cutplanes: (a) and (c) depict the result directly delivered by CST whereas (b) and (d) show the result delivered by SSC. The respective colorbars are presented in Figure 5. Note that the waveguides for the absorption of higher-order modes are elongated by $\lambda/4$ in the direct run to emulate perfect magnetic conducting boundary conditions with perfect electric boundary conditions.

ing subsection is focused on mode $n = 888$ to conduct a plausibility analysis of SSC.

Comparison of SSC with Direct Computation

Figure 3 depicts the absolute value of the electric field distribution of mode $n = 888$ in the BESSY VSR cavity chain. The mode has a comparably large coupling impedance $(r/Q)_{888}^{\mathrm{SSC}} \approx 7.7298\,\Omega$ and its frequency $f_{888}^{\mathrm{SSC}} = 2.9899\,\mathrm{GHz}$ is close to the $\Delta f = 250\,\mathrm{MHz}$ harmonics of the beam current. Thus, this mode is of interest although it is expected to have a small external quality factor because of its strong coupling to the higher-order mode absorbers.

Figure 3 shows that the field energy of the mode is confined across two segments, namely at one $1.75\,\mathrm{GHz}$ resonator and at the collimating shielded bellow. Therefore, this eigenmode is suitable to compare the SSC result with a direct eigenmode computation using CST [16]. The direct eigenmode computation is performed for a geometry comprising three cells of the $1.75\,\mathrm{GHz}$ resonator with higher-order mode couplers, the collimating shielded bellow and one cell of the next $1.75\,\mathrm{GHz}$ resonator with fundamental power coupler and input coupler. Please refer Figure 4(a) and Figure 4(c) for cutplanes of the structure considered by the direct eigen-

mode computation. Note that the higher-order waveguide absorbers are slightly elongated by $\lambda/4 = c/4/\sqrt{f_{888}^2 - f_{\mathrm{co}}^2}$, because CST does not allow to specify perfect magnetic boundary conditions within the computational domain. Here, λ is the wavelength in the higher-order mode waveguide coupler and f_{co} the cutoff frequency of the fundamental waveguide mode. A tetrahedral mesh with 218,444 tetrahedrons is used to generate a discrete representation of Eq. (1) for the substructure depicted in 4(a) and Figure 4(c). The tetrahedral mesh is chosen because it is more suitable to discretize the smooth curvatures of the geometry. Moreover, in general, the properties of the eigenmodes should neither depend on the discretization (tetrahedral or hexahedral) nor on the numerical approach (direct or SSC). The eigenmode solver of CST [16] is requested to search for 10 modes with resonant frequencies larger than $2.98\,\mathrm{GHz}$. The computational time required to determine these 10 eigenmodes is approximately 13 min on an Intel(R) Xeon(R) CPU E5-2687W @ 3.4 GHz with 256 GB of RAM using Windows Server 2012.

The resonant frequency arising from the direct computation is $f_{888}^{\mathrm{CST}} = 2.9863\,\mathrm{GHz}$, so that the relative difference in the frequency between direct computation and SSC amounts to less than 1.2×10^{-3}. The coupling impedance delivered by the direct computation amounts to $(r/Q)_{888}^{\mathrm{CST}} = 8.8095\,\Omega$, so that a relative difference of $\approx 1.2 \times 10^{-1}$ results.

SUMMARY AND CONCLUSION

The SSC scheme allows for the determination of eigenmodes of long chains of cavities using workstations. The key of the method is the combination of non-overlapping domain decomposition with model-order reduction. The scheme allows for the creation of eigenmode compendia, which systematically comprise field distributions, resonant frequencies, coupling impedances, and quality factors.

In addition to the various comparisons of SSC results with direct computations for test structures (refer for instance to [5, 6, 8, 9]), this contribution presents a comparison using another structure. The confinement of the studied mode in two segments of the chain allows for a comparison with a direct computation using CST.

As a central result, the resonant frequency agrees very well for this mode and the coupling impedance agrees reasonably well. The differences are attributed to the different discretization techniques (tetrahedral vs. hexahedral mesh) and the different numerical approaches (direct vs. SSC).

TUPAG01

ACKNOWLEDGEMENTS

APPENDIX

Figure 5(a) presents the colorbar for the absolute values of the electric field strength delivered by SSC whereas Figure 5(b) depicts the corresponding colorbar for the direct computation using CST.
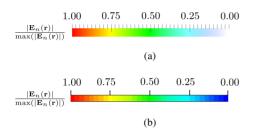

Figure 5: (a) Colorbar for SSC field plots. (b) Colorbar for CST field plots.

REFERENCES

[1] R. V. Beeumen *et al.*, "Computing resonant modes of accelerator cavities by solving nonlinear eigenvalue problems via rational approximation," *Journal of Computational Physics*, vol. 374, pp. 1031–1043, 2018, ISSN: 0021-9991.

[2] I. R. R. Shinton, R. M Jones, Z. Li, and P. Zhang, "Simulations of Higher Order Modes in the ACC39 Module of FLASH," in *Proceedings of International Particle Accelerator Conference 2012*, New Orleans, Louisiana, USA, May 2012, pp. 1900–1902.

[3] K. Ko et al., "Advances in Parallel Electromagnetic Codes for Accelerator Science and Development," in *Proceedings of the Linear Accelerator Conference 2010*, Tsukuba, Japan, 2010, pp. 1028–1032.

[4] F. Yaman, W. Ackermann, and T. Weiland, "Comparison of Eigenvalue Solvers for Large Sparse Matrix Pencils," in *Proceedings of the 11th International Computational Accelerator Physics Conference 2012*, Rostock-Warnemünde, Germany, 2012, pp. 287–289.

[5] T. Flisgen, H.-W. Glock, and U. van Rienen, "Compact Time-Domain Models of Complex RF Structures based on the real Eigenmodes of Segments," *IEEE Transactions on Microwave Theory and Techniques*, vol. 61, no. 6, pp. 2282–2294, 2013. DOI: 10.1109/TMTT.2013.2260765.

[6] T. Flisgen, "Compact state-space models for complex superconducting radio-frequency structures based on model order reduction and concatenation methods," available as CERN-ACC-2015-0145, PhD thesis, University of Rostock, 2015.

[7] T. Flisgen *et al.*, "Eigenmode Compendium of the Third Harmonic Module of the European XFEL Computed by SSC," *Physical Review Accelerators and Beams*, vol. 20, no. 4, Apr. 2017. DOI: 10.1103/PhysRevAccelBeams.20.042002.

[8] T. Flisgen, J. Heller, and U. van Rienen, "Computation of Eigenmodes in Long and Complex Accelerating Structures by Means of Concatenation Strategies," in *Proceedings of the 5th International Particle Accelerator Conference 2014 (IPAC 2014)*, Dresden, Germany, 2014, pp. 947–949.

[9] J. Heller, T. Flisgen, and U. van Rienen, "Computational Benefits Using an Advanced Concatenation Scheme Based on Reduced Order Models for RF Structures," *Physics Procedia*, vol. 79, pp. 38–45, 2015. DOI: 10.1016/j.phpro.2015.11.060.

[10] T. Weiland, "A Discretization Method for the Solution of Maxwell's Equations for Six-Component Fields," *Electronics and Communications AEUE*, vol. 31, no. 3, pp. 116–120, 1977.

[11] U. Rienen, *Numerical Methods in Computational Electrodynamics: Linear Systems in Practical Applications*. Berlin, Germany: Springer, 2001, ISBN: 3540676295.

[12] T. Wittig, *Zur Reduzierung der Modellordnung in elektromagnetischen Feldsimulationen*. Cuvillier Verlag, 2004, ISBN: 9783865372086.

[13] T. Wittig, R. Schuhmann, and T. Weiland, "Model order reduction for large systems in computational electromagnetics," *Linear Algebra and its Appl.*, vol. 415, no. 2 - 3, pp. 499–530, Jun. 2006.

[14] A. C. Antoulas, *Approximation of Large-Scale Dynamical Systems*. Philadelphia, PA, USA: Society for Industrial and Applied Mathematics, 2005, ISBN: 9780898718713.

[15] J. Heller and U. van Rienen, "Report on SSC calculations for BESSY VSR," University of Rostock, Internal Report, 2017.

[16] CST AG, *CST STUDIO SUITE 2018*. Bad Nauheimer Str. 19, 64289 Darmstadt, Germany.

[17] G. Wüstefeld, A. Jankowiak, J. Knobloch, and M. Ries, "Simultaneous Long and Short Electron Bunches in the BESSY II Storage Ring," in *2nd International Particle Accelerator Conference (IPAC'11), San Sebastián, Spain*, 2011.

[18] A. Jankowiak et al., "Technical Design Study BESSY VSR," Helmholtz-Zentrum Berlin, Internal Report, 2015.

[19] A. Vélez et al., "The SRF Module Developments for BESSY VSR," in *8th International Particle Accelerator Conference (IPAC'17), Copenhagen, Denmark*, 2017.

[20] T. Flisgen, H.-W. Glock, and A. Tsakanian, "Estimation of Dielectric Losses in the BESSY VSR Warm Beam Pipe Absorbers," in *9th International Particle Accelerator Conference (IPAC'18), Vancouver, BC, Canada*, 2018.

[21] The MathWorks Inc., *Matlab version r2015b*.

[22] A. Henderson and J. Ahrens, *The Paraview guide: a parallel visualization application*. New York: Kitware, Inc., 2004, ISBN: 1930934149.

[23] J. Heller, "Numerical simulation of electromagnetic felds in complex multi-cavity superconducting radio frequency resonators," PhD thesis, Universität Rostock, 2018.

[24] H. W. Pommerenke, J. Heller, and U. Rienen, "Efficient Computation of Lossy Higher Order Modes in Complex SRF Cavities Using Reduced Order Models and Nonlinear Eigenvalue Problem Algorithms," in *Proceedings of the 13th International Computational Accelerator Physics Conference 2018*, Key West, Florida, USA, 2018, this conference.